CANCER

Engineered T cells secreting anti-BCMA T cell engagers control multiple myeloma and promote immune memory in vivo

Laura Díez-Alonso[1,2,3]†, Aïda Falgas[4,5]†, Javier Arroyo-Ródenas[1,2,3]†, Paola A. Romencín[4], Alba Martínez[4], Marina Gómez-Rosel[1,2,3], Belén Blanco[1,2,3,5], Anaïs Jiménez-Reinoso[1,2,3], Andrea Mayado[6,7,8], Alba Pérez-Pons[6,7,8], Óscar Aguilar-Sopeña[9,10], Ángel Ramírez-Fernández[1,2,3], Alejandro Segura-Tudela[1,2,3], Lorena Perez-Amill[11], Antonio Tapia-Galisteo[1,2,3], Carmen Domínguez-Alonso[1,2,3], Laura Rubio-Pérez[1,2,3,12], Maria Jara[6,7,8], Francesc Solé[4], Oana Hangiu[1,2], Laura Almagro[9,10], Ángela Albitre[13,14], Petronila Penela[13,14], Laura Sanz[15], Eduardo Anguita[16,17], Antonio Valeri[18,19], Almudena García-Ortiz[18,19], Paula Río[5,20,21,22], Manel Juan[5,11,23,24,25], Joaquín Martínez-López[5,18,19], Pedro Roda-Navarro[9,10], Beatriz Martín-Antonio[26], Alberto Orfao[6,7,8], Pablo Menéndez[4,5,7,27,28], Clara Bueno[4,5,7]*, Luis Álvarez-Vallina[1,2,3,12]*

Multiple myeloma is the second most common hematological malignancy in adults and remains an incurable disease. B cell maturation antigen (BCMA)–directed immunotherapy, including T cells bearing chimeric antigen receptors (CARs) and systemically injected bispecific T cell engagers (TCEs), has shown remarkable clinical activity, and several products have received market approval. However, despite promising results, most patients eventually become refractory and relapse, highlighting the need for alternative strategies. Engineered T cells secreting TCE antibodies (STAb) represent a promising strategy that combines the advantages of adoptive cell therapies and bispecific antibodies. Here, we undertook a comprehensive preclinical study comparing the therapeutic potential of T cells either expressing second-generation anti-BCMA CARs (CAR-T) or secreting BCMAxCD3 TCEs (STAb-T) in a T cell–limiting experimental setting mimicking the conditions found in patients with relapsed/refractory multiple myeloma. STAb-T cells recruited T cell activity at extremely low effector-to-target ratios and were resistant to inhibition mediated by soluble BCMA released from the cell surface, resulting in enhanced cytotoxic responses and prevention of immune escape of multiple myeloma cells in vitro. These advantages led to robust expansion and persistence of STAb-T cells in vivo, generating long-lived memory BCMA-specific responses that could control multiple myeloma progression in xenograft models, outperforming traditional CAR-T cells. These promising preclinical results encourage clinical testing of the BCMA-STAb-T cell approach in relapsed/refractory multiple myeloma.

INTRODUCTION

Multiple myeloma (MM) is the second most common hematological malignancy in adults (*1*, *2*), and although recent therapeutic strategies have markedly improved survival (*3*), relapsed/refractory (R/R) MM remains an incurable cancer. Patients who are refractory to five treatment lines have a median overall survival of less than 6 months (*4*). Redirecting T cell activity toward cancer cells through targeting a cell surface tumor-associated antigen (TAA), such as by membrane-anchored chimeric antigen receptors (CARs) or soluble bispecific (anti-TAA × anti-CD3) T cell–engaging (TCE) antibodies, represents

[1]Cancer Immunotherapy Unit (UNICA), Department of Immunology, Hospital Universitario 12 de Octubre, 28041 Madrid, Spain. [2]Immuno-Oncology and Immunotherapy Group, Instituto de Investigación Sanitaria Hospital 12 de Octubre (imas12), 28041 Madrid, Spain. [3]H12O-CNIO Cancer Immunotherapy Clinical Research Unit, Spanish National Cancer Research Centre (CNIO), 28029 Madrid, Spain. [4]Josep Carreras Leukaemia Research Institute, 08036 Barcelona, Spain. [5]Red Española de Terapias Avanzadas (TERAV), Instituto de Salud Carlos III, 28029 Madrid, Spain. [6]Cancer Research Center (IBMCC, USAL-CSIC), Department of Medicine and Cytometry Service (NUCLEUS), Universidad de Salamanca, 37007 Salamanca, Spain. [7]Centro de Investigación Biomédica en Red-Oncología (CIBERONC), Instituto de Salud Carlos III, 28029 Madrid, Spain. [8]Biomedical Research Institute of Salamanca (IBSAL), 37007 Salamanca, Spain. [9]Department of Immunology, Ophthalmology and ENT, School of Medicine, Universidad Complutense, 28040 Madrid, Spain. [10]Lymphocyte Immunobiology Group, Instituto de Investigación Sanitaria 12 de Octubre (imas12), 28041 Madrid, Spain. [11]Institut d'Investigacions Biomèdiques August Pi i Sunyer (IDIBAPS), Hospital Clinic de Barcelona, 08036 Barcelona, Spain. [12]Chair for Immunology UFV/Merck, Universidad Francisco de Vitoria (UFV), Pozuelo de Alarcón, 28223 Madrid, Spain. [13]Centro de Biología Molecular Severo Ochoa CSIC-UAM, 28049 Madrid, Spain. [14]Instituto de Investigación Sanitaria La Princesa, 28006 Madrid, Spain. [15]Molecular Immunology Unit, Hospital Universitario Puerta de Hierro Majadahonda, Majadahonda, 28222 Madrid, Spain. [16]Department of Medicine, Medical School, Universidad Complutense de Madrid, 28040 Madrid, Spain. [17]Department of Hematology, IML, IdISSC, Hospital Clínico San Carlos, 28040 Madrid, Spain. [18]H12O-CNIO Hematological Malignancies Clinical Research Unit, Spanish National Cancer Research (CNIO), 28029 Madrid, Spain. [19]Department of Hematology, Hospital Universitario 12 de Octubre-Universidad Complutense, Instituto de Investigación Sanitaria Hospital 12 de Octubre (imas12), 28041 Madrid, Spain. [20]Division of Hematopoietic Innovative Therapies, Biomedical Innovation Unit, Centro de Investigaciones Energéticas Medioambientales y Tecnológicas (CIEMAT), 28040 Madrid, Spain. [21]Centro de Investigación Biomédica en Red de Enfermedades Raras (CIBERER), Instituto de Salud Carlos III, 28029 Madrid, Spain. [22]Instituto de Investigación Sanitaria Fundación Jiménez Díaz, Universidad Autónoma de Madrid (IIS-FJD, UAM), 28040 Madrid, Spain. [23]Servei d'Immunologia, Hospital Clínic de Barcelona, 08036 Barcelona, Spain. [24]Plataforma Immunoterapia, Hospital Sant Joan de Deu, 08950 Barcelona, Spain. [25]Universitat de Barcelona, 08007 Barcelona, Spain. [26]Department of Experimental Hematology, Instituto de Investigación Sanitaria Fundación Jiménez Diaz, (IIS-FJD), Universidad Autónoma de Madrid, 28040 Madrid, Spain. [27]Department of Biomedicine, School of Medicine, Universitat de Barcelona, 08007 Barcelona, Spain. [28]Institució Catalana de Recerca i Estudis Avançats (ICREA), 08010 Barcelona, Spain.
*Corresponding author. Email: cbueno@carrerasresearch.org (C.B.); lalvarezv@ext.cnio.es, lav.imas12@h12o.es (L.Á.-V.)
†These authors contributed equally to this work.

a promising approach for several hematological malignancies (*5*), including MM (*6*, *7*). B cell maturation antigen (BCMA), also referred to as CD269 or TNFRSF17, is a member of the tumor necrosis factor receptor (TNFR) superfamily, which regulates B cell proliferation, survival, and differentiation to plasma cells (PCs) by binding to a proliferation-inducing ligand (APRIL) and B cell activating factor (BAFF) (*8*, *9*). BCMA is an attractive target for T cell–redirecting strategies because it is almost exclusively expressed on plasmablasts and PCs and is overexpressed on malignant PCs (*10*). BCMA is undetectable in naïve and memory B lymphocytes, hematopoietic stem cells, and most nonhematological normal tissues (*11*).

BCMA-targeted T cell–redirecting immunotherapies have been extensively evaluated at the preclinical level and are under active clinical investigation in R/R MM (*12*, *13*). Adoptive cell therapy (ACT) with BCMA-specific CAR-T cells has shown unprecedented results with excellent safety profiles, leading to approval by the US Food and Drug Administration (FDA) and the European Medicines Agency (EMA) of two second-generation CAR-T cell products (idecabtagene vicleucel and ciltacabtagene autoleucel) (*14*, *15*). These results have also been confirmed in an additional clinical study of patients treated with BCMA-specific CAR-T cells (*16*). Moreover, the FDA recently approved the BCMA-specific TCEs teclistamab (*17*) and elranatamab (*18*). However, despite the encouraging results obtained with BCMA-specific immunotherapies, most patients eventually relapse or show disease progression (*15*), highlighting the need for refined therapeutic strategies.

In addition to its membrane-anchored form, BCMA has a soluble form (sBCMA) derived from the natural shedding of membrane BCMA through γ-secretase activity, and serum sBCMA concentrations correlate with disease progression and poor treatment outcome (*19*). BCMA shedding is an obstacle to BCMA-targeted therapies both by reducing cell surface BCMA density and by acting as a decoy that neutralizes the activity of redirected T cells, as reported for BCMA-specific CAR-T cells (*20*); however, the impact on TCE-based therapies is considerably lower (*21*). CAR-T cells may have some advantages over systemically administered TCEs, such as the expansion and persistence of adoptively transferred CAR-T cells, creating a reservoir of memory cells that could provide long-term antitumor response (*22*). In contrast, the efficacy of TCEs would be determined by drug exposure, and it is unlikely that a strategy based on their systemic administration would generate a pool of long-term memory antitumor T cells once the drug is withdrawn (*23*).

An emerging T cell–redirecting strategy that uses both ACTs and bispecific antibodies, which we refer to as STAb (secretion of TCE antibodies) (*5*, *24*), relies on the in vivo production of TCEs by engineered T cells (*25*–*27*). Sustained in vivo TCE secretion results in effective serum concentrations of the TCE (*28*). Furthermore, expansion and persistence of adoptively transferred STAb-T cells (*29*, *30*), as well as polyclonal recruitment of both gene-modified STAb-T cells and unmodified bystander T cells to the tumor microenvironment (TME), can lead to substantially increased antitumor responses (*29*–*31*). The therapeutic potential of STAb-T cells has been demonstrated in B cell (*29*–*32*) and T cell hematological malignancies (*30*). Here, we report the generation of STAb-T cells secreting an anti-BCMA TCE and demonstrate their superior efficacy over BCMA-specific CAR-T cells under T cell–limiting conditions simulating those found in patients with multitreated MM.

RESULTS

STAb-T cells efficiently secrete anti-BCMA TCEs and promote the formation of canonical immunological synapses

We generated a tandem anti-BCMA × anti-CD3 bispecific antibody (BCMA-TCE) by fusing the clinically validated anti-BCMA J22.9 scFv (*33*) and the anti-CD3 OKT3 scFv through a G_4S sequence (Fig. 1, A and B), which was cloned under the control of the EF1α promoter into a T2A-based bicistronic lentiviral vector expressing the tdTomato (tdTo) reporter protein (Fig. 1C) (*29*). The vector encoding an anti-BCMA second-generation (4-1BB–CD3ζ) CAR (Fig. 1D) using the same anti-BCMA scFv (BCMA-CAR) (Fig. 1, E and F) has been described previously (*20*). Comparable transduction efficiencies were observed according to the percentage of $tdTo^+$ cells in Jurkat T cells transduced with BCMA-TCE– or BCMA-CAR–encoding lentiviral vectors (J-STAb-T and J-CAR-T, respectively) (fig. S1A). The intracellular expression of BCMA-TCE and its interaction with CD3 on the surface of Jurkat T cells (a process called "CD3 decoration") were verified with an anti–His-tag monoclonal antibody (mAb) (fig. S1B), and the cell surface expression of BCMA-CAR was confirmed after staining with BCMA-Fc (fig. S1C). The intracellular expression of both BCMA-CAR and BCMA-TCE (fig. S1, D and E) and the extracellular secretion of BCMA-TCE (fig. S1F) were further confirmed by Western blotting. The secreted BCMA-TCE specifically recognized plastic-immobilized BCMA-Fc (fig. S1G) and induced CD69 expression in cocultures of J-STAb-T cells with $BCMA^+$ U266 cells (fig. S1H) at frequencies similar to those obtained in cocultures with J-CAR-T cells (fig. S1I). The secretion of BCMA-TCE by J-STAb-T cells is not reduced in situations of persistent activation and up-regulation of exhaustion markers (fig. S1, J and K).

Immunofluorescence assays were performed to study the assembly of the immunological synapse and early signaling by staining for filamentous actin (F-actin), as a marker of the distal supramolecular activation clusters, and phosphotyrosine (pTyr), respectively. CAR-T and STAb-T Jurkat cells were cocultured with U266 cells for 15 min to allow the assembly of the immunological synapse, and superantigen-E (SEE)–loaded Raji cells cocultured with nontransduced (NT) Jurkat T cells were used as a positive control. Confocal microscopy images showed that both J-CAR-T and J-STAb-T cells induced the assembly of the immunological synapse with U266 cells (Fig. 1G). F-actin and pTyr were observed to polarize toward the immunological synapse (Fig. 1G). Although the pTyr ratio did not vary, the F-actin polarization ratio was slightly lower in BCMA-CAR–mediated immunological synapse than in BCMA-TCE–mediated immunological synapse (fig. S2, A to D). Consistent with previous reports (*29*–*34*), the typical central actin-cleared area of the immunological synapse was not properly organized in J-CAR-T in comparison with J-STAb-T cells (Fig. 1G and fig. S2E).

STAb-T cells induce specific cytotoxic responses at low effector:target ratios

Primary T cells were transduced with BCMA-CAR– or BCMA-TCE–encoding lentiviral vectors with comparable transduction efficiencies, ranging from 17 to 30% (average 22.7 and 21%, respectively) (Fig. 1H and fig. S3A). No differences were observed in the CD4:CD8 ratio between $BCMA\text{-}CAR^+$ and $BCMA\text{-}TCE^+$ cells (fig. S3B), with comparable proportions of naïve, central memory, effector memory, and effector subsets among NT-T, CAR-T, and STAb-T cells, and an overall prevalence of effector T cells (fig. S3C).

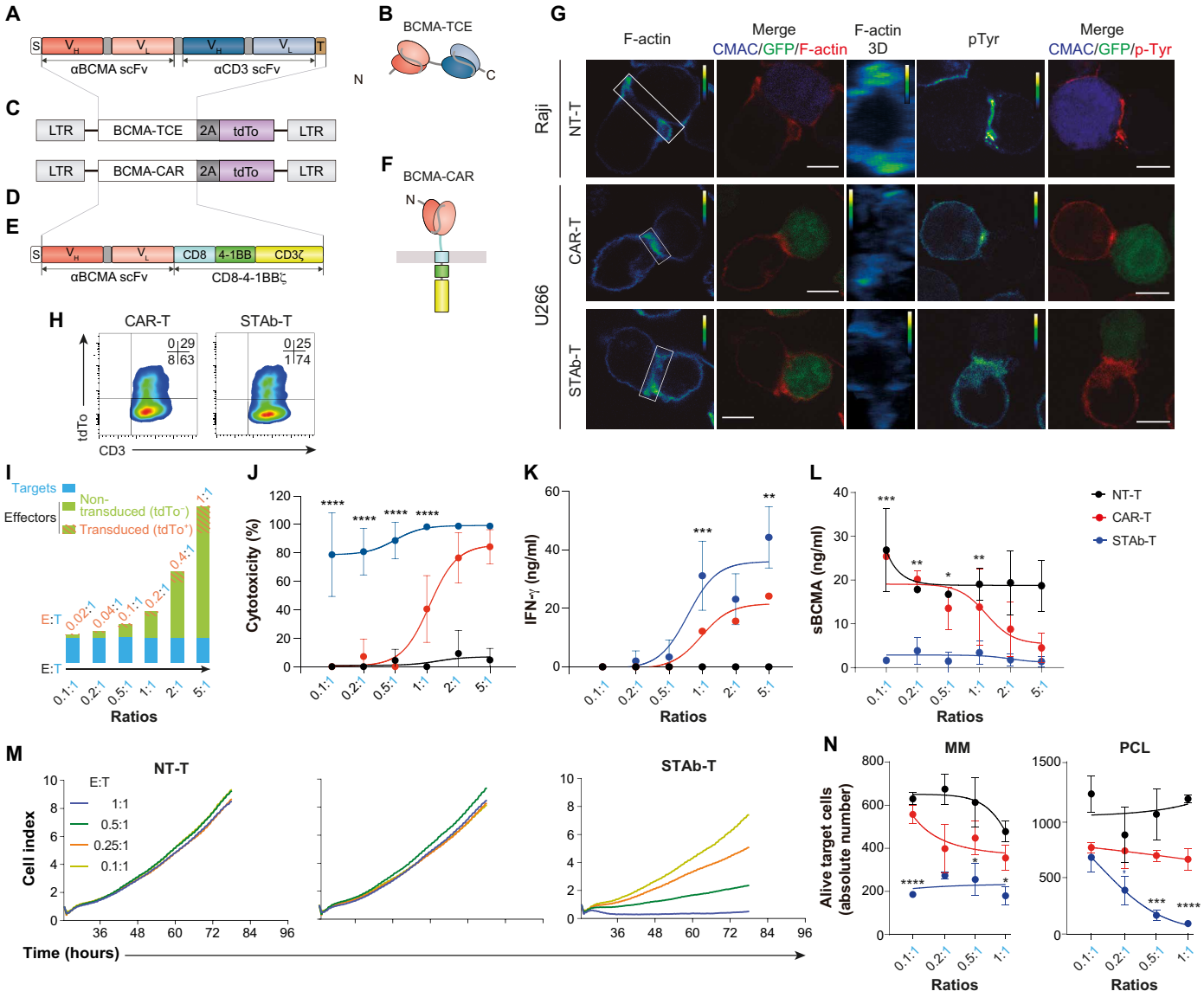

Fig. 1. BCMA-specific STAb-T cells show enhanced cytotoxic activity in vitro and promote canonical immunological synapses compared to CAR-T cells. (**A** and **B**) Schematic diagrams showing the genetic (A) and domain structure (B) of the bispecific anti-BCMA × anti-CD3 antibody (BCMA-TCE), bearing a signal peptide from the human k light chain signal peptide (white box), the anti-BCMA (J22.9) scFv gene (orange boxes), the anti-CD3 (OKT3) scFv gene (blue boxes), and a His tag (brown box). (**C**) BCMA-TCE–encoding lentiviral vector, containing the tdTo gene after the 2A sequence from *Thosea asigna* virus. (**D**) A similar lentiviral vector containing the tdTo gene and the 2A sequence was designed for cloning the anti-BCMA CAR (BCMA-CAR). (**E** and **F**) Genetic (E) and domain structure (F) of the second-generation CAR-BCMA used in this study. (**G**) Topology of the immunological synapse induced by Jurkat CAR-T and STAb-T cells incubated with BCMA$^+$ U266 cells. Representative conjugates are shown. Conjugates of NT Jurkat T cells (NT-T) and SEE-loaded Raji cells are used to show the organization of actin at a canonical immunological synapse. pTyr and F-actin distribution to the immunological synapse of a confocal section are displayed in pseudocolor. Red pTyr or F-actin merged with blue CMAC (7-amino-4-chloromethylcoumarin) or green fluorescent protein (for target cell identification) are shown. Scale bar, 5 μm. The surface interface of the interaction (identified by a white rectangle) obtained by 3D-confocal microscopy is shown for F-actin as pseudocolor. (**H**) Percentage of reporter protein expression (tdTo) in primary CAR-T and STAb-T cells. One representative transduction out of eight independent transductions performed is shown. (**I**) Schematic representation of the E:T ratios used in cytotoxicity experiments using U266^{Luc} as target, showing the proportion of transduced (CAR-T or STAb-T) and NT effector T cells. (**J**) Cytotoxicity induced at decreasing E:T ratios of NT-T, CAR-T, or STAb-T cells from the same donor cocultured with U266^{Luc} target cells for 48 hours, measured by adding D-luciferin to detect bioluminescence. (**K** and **L**) IFN-γ secretion (K) and sBCMA concentrations (L) were determined by ELISA. Data in (J) to (L) are mean ± SD of one experiment performed in triplicate ($n = 3$). Significance was calculated by two-way ANOVA test corrected with a Tukey's multiple comparisons test. (**M**) Real-time cell cytotoxicity assay with HEK293^{BCMA} target cells cocultured with NT-T, CAR-T, or STAb-T cells at the indicated E:T ratios. Cell index values were determined every 15 min for 78 hours using an impedance-based method. One representative experiment performed in duplicate is shown. (**N**) Cytotoxicity induced by NT-T, CAR-T, or STAb-T cells from the same donor cocultured in triplicates at the indicated E:T ratios with primary human BM cells from a patient with MM and PBMCs from a patient with PCL. The number of alive (DAPI$^-$) target MM or PCL cells was determined after 24 hours. Significance in (N) was calculated by two-way ANOVA test corrected with a Tukey's multiple comparisons test. *$P < 0.05$, **$P < 0.01$, ***$P < 0.001$, ****$P < 0.0001$.

To study their specificity and killing efficiency, CAR-T and STAb-T effector cells were cocultured with BCMA$^+$ (U266^{Luc}) or BCMA$^-$ (K562^{Luc}) target cells at different effector:target (E:T) ratios. To better understand the contribution of transduced (tdTo$^+$) effector T cells (CAR-T$^+$ and STAb-T$^+$), and NT (tdTo$^-$) effector T cells (CAR-T$^-$ and STAb-T$^-$) in the functional responses, both total E:T and the transduced E:T ratios are depicted in Fig. 1I. CAR-T cells exhibited substantial cytotoxicity (≥80%) at higher ratios, which was reduced at E:T ratios below 1:1 (transduced E:T 0.2:1) (Fig. 1, I and J). In contrast, STAb-T cells induced, on average, ≥80% specific cytotoxicity at all ratios tested, even at the lowest ratio corresponding to 1 T cell per 10 target cells (Fig. 1, I and J). In both CAR-T and STAb-T cell cocultures, interferon-γ (IFN-γ) secretion was detected at E:T ratios above 1:1. In CAR-T cell cocultures, there was a correspondence between cytotoxic activity and IFN-γ secretion; however, in STAb-T cell cocultures at very low E:T ratios, maximal cytotoxicity was reached without detectable production of IFN-γ (Fig. 1K). No cytotoxicity or IFN-γ secretion was observed when K562 cells were used as targets (fig. S4, A and B). U266 cells produce substantial amounts of sBCMA under basal conditions (fig. S5), and as shown in Fig. 1L, in cocultures with CAR-T cells, sBCMA concentrations were reduced only at the higher E:T ratios. In contrast, in cocultures with STAb-T cells, sBCMA concentrations were nearly undetectable in all conditions studied (Fig. 1L). sBCMA concentrations were not modified in cocultures with NT-T cells (Fig. 1L).

We next assessed the cytotoxic activity under stressed conditions (≤1:1 E:T) in an impedance-based real-time assay against nontransfected and BCMA-transfected human embryonic kidney (HEK) 293 cells (HEK293 and HEK293^{BCMA}, respectively). In cocultures with HEK293^{BCMA} cells, which express substantial amounts of cell surface BCMA and sBCMA secretion (fig. S6, A and B), STAb-T cells were found to reduce BCMA$^+$ target cell viability even at 0.25:1 E:T ratio, whereas CAR-T cells showed no cytotoxic effect at any of the analyzed ratios (Fig. 1M). HEK293^{BCMA} cells cocultured with NT-T cells (Fig. 1M) or HEK293 cells cocultured with NT-T, CAR-T, or STAb-T cells displayed similar viability kinetics to those of target cells cultured alone (fig. S7, A and B). To study the activity of CAR-T and STAb-T cells under stressed conditions (≤1:1 E:T) in a clinically relevant context, we designed ex vivo cytotoxicity assays using bone marrow (BM) cells of a patient with MM (fig. S8A) and peripheral blood mononuclear cells (PBMCs) of a patient with plasma cell leukemia (PCL) (fig. S8B) as target cells. After 24 hours of coculture, STAb-T cells were able to eliminate 70% of the MM-derived target cells (CD38$^+$CD138$^+$) in all analyzed E:T ratios (from 1:1 to 0.1:1) (Fig. 1N). CAR-T cells were less effective, with 30% of MM cell lysis at the higher E:T ratios (Fig. 1N). Against PCL-derived target cells, STAb-T cells were similarly more effective than CAR-T cells and were able to eliminate nearly 100% of the PCL cells at the 0.5:1 and 1:1 E:T ratios (Fig. 1N).

STAb-T cells recruit bystander T cells and prevent tumor escape in vitro more efficiently than CAR-T cells

To investigate the ability of STAb-T cells to recruit bystander T cells, we cocultured activated T (A-T) cells (NT-T, CAR-T, or STAb-T) or mixtures of A-T and freshly isolated nonactivated T (NA-T) cells from the same healthy donor with either BCMA$^+$ (U266^{Luc} or ARP1^{Luc}) or BCMA$^-$ (K562^{Luc}) targets. The A-T and target cells were mixed at decreasing A-T:target ratios (from 1:1 to 0.0001:1) but adding NA-T cells to keep a constant 1:1 E:T ratio (Fig. 2A). In cocultures with U266^{Luc} cells, STAb-T cells exhibited 100% cytotoxicity even at the 0.01:1 A-T:target ratio, whereas CAR-T cells only induced 60% cytotoxicity at the 1:1 ratio, which was severely reduced at the 0.1:1 ratio (Fig. 2B). No cytotoxicity or IFN-γ secretion was observed when mixtures of A-T and NA-T cells were cocultured with K562^{Luc} cells (fig. S9, A to C). In cocultures with ARP1^{Luc} cells, CAR-T cells displayed only 30% cytotoxic activity at the 1:1 A-T:target ratio, whereas STAb-T cells showed ≥90% specific cytotoxicity even at the 0.1:1 ratio (fig. S10A). In these experimental conditions, there was a correspondence between cytotoxic activity and IFN-γ secretion (Fig. 2C and fig. S10B). To further demonstrate that STAb-T cells were able to recruit bystander NA-T cells, U266 ^{Luc} or K562^{Luc} target cells were plated with NA-T cells in the bottom chamber of a transwell system, and NT-T, STAb-T, or CAR-T cells were plated in the insert well (Fig. 2D). Cytotoxicity and IFN-γ secretion were fully dependent on the presence of STAb-T cells in the insert well and U266 ^{Luc} in the bottom chamber, indicating that secreted BCMA-TCEs crossed the transwell filter and effectively redirected the effector activity of NA-T cells to BCMA$^+$ cells (Fig. 2, E and F, and fig. S11). Next, we evaluated the ability of CAR-T and STAb-T cells to prevent tumor escape under stressed conditions in cocultures with U266 cells at decreasing E:T ratios (from 1:1 to 0.06:1). CAR-T cells did not control the growth of MM cells at any of the ratios studied (Fig. 2G and fig. S12). These results are similar to those obtained with ARP1 cells (fig. S13, A and B). The difference with respect to that reported in previous works with the same CAR construct (*20*) may be attributable to the lower transduction frequencies achieved in this work (around 20%). However, STAb-T cells were able to control the growth of U266 cells even at the 0.25:1 ratio (Fig. 2G and fig. S12) and that of ARP1 cells at a 0.5:1 ratio (fig. S13, A and B).

sBCMA has no impact on STAb-T–mediated cytotoxicity

To study the effect of sBCMA on effector functions, we cocultured CAR-T and STAb-T cells with U266^{Luc} cells at a 1:1 E:T ratio in the presence of increasing concentrations (from 0 to 5 μg/ml) of BCMA-Fc chimera (BCMA-Fc). The cytotoxic activity of CAR-T cells decreased as the concentration of sBCMA exceeded 0.1 μg/ml with total inhibition at concentrations of 5 μg/ml (Fig. 2H). By contrast, the cytotoxicity of STAb-T cells was not compromised and remained at 100% at all concentrations of BCMA-Fc studied (Fig. 2H). IFN-γ secretion was reduced with increasing BCMA-Fc concentration in both STAb-T and CAR-T cells (Fig. 2I), consistent with the lower threshold for cytolysis compared with cytokine production.

STAb-T cells are more effective than CAR-T cells in a murine model of MM

To study the in vivo effect of STAb-T cells in a xenograft model of MM, nonobese diabetic scid gamma (NSG) mice were intravenously infused with 1×10^6 U266^{Luc} cells, followed 3 days later by intravenous injection of phosphate-buffered saline (PBS; control), or T cells. Three groups of mice received 5×10^6 NT-T, CAR-T, or STAb-T cells, referred to as the standard condition, whereas two other groups were inoculated with a limited number (3×10^6) of CAR-T or STAb-T cells, referred to as the therapeutic limiting dose (TLD) condition. In both conditions, the percentage of transduced CAR-BCMA$^+$ or TCE-BCMA$^+$ cells was 20% (Fig. 3A). Bioluminescence imaging (BLI) and body weight measurement were performed at the indicated time points to assess MM progression and xenogeneic graft-versus-host disease (Fig. 3, B to E). Control and

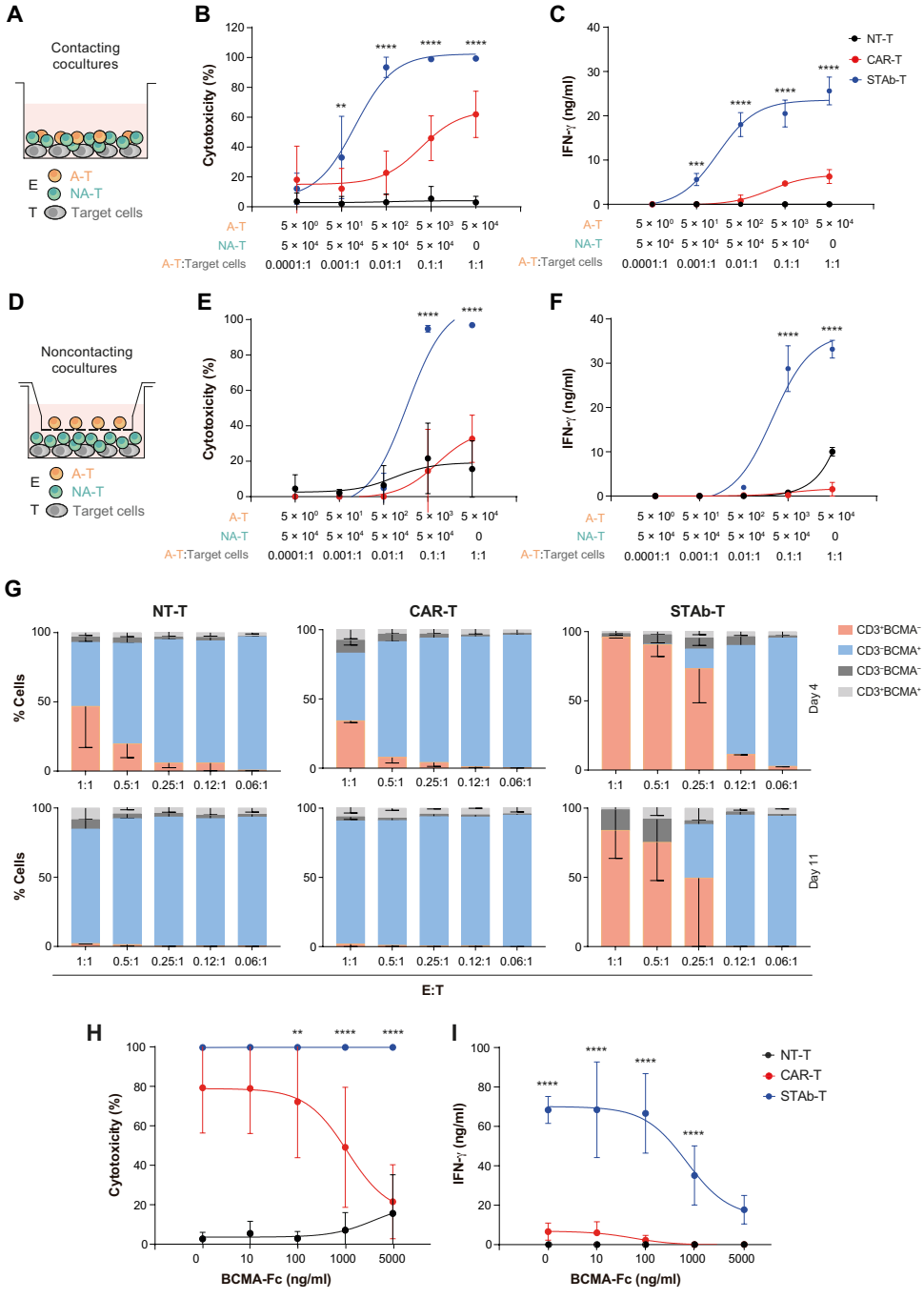

Fig. 2. STAb-T cells recruit bystander T cells and prevent tumor escape in vitro. (**A**) Schematic representation of the direct contact coculture system to study the ability of CAR-T and STAb-T cells to recruit bystander T cells. (**B**) Cytotoxic activity induced by varying numbers of A-T cells (NT-T, CAR-T, or STAb-T) and freshly isolated NA-T cells from the same donor cocultured with U266^{Luc} target cells for 48 hours, maintaining a constant 1:1 E:T ratio, and measured by adding D-luciferin to detect bioluminescence. Data in (B) are mean ± SD of three independent experiments with triplicates (n = 9). (**C**) IFN-γ secretion was determined by ELISA. Data in (C) are mean ± SD of one experiment with triplicates (n = 3). Significance was calculated by two-way ANOVA test corrected with a Tukey's multiple comparisons test. (**D**) Schematic representation of the noncontacting transwell system used. U266^{Luc} target cells and NA-T cells were plated in the bottom well and A-T cells (NT-T, CAR-T, or STAb-T) in the insert well. (**E** and **F**) After 48 hours, the percentage of cytotoxicity was determined by luciferase assay (E), and IFN-γ secretion was measured by ELISA (F). Data are mean ± SD of triplicates from one experiment (n = 3). Significance was calculated by two-way ANOVA test corrected with a Tukey's multiple comparisons test. (**G**) Myeloma escape from immune pressure. U266 cells were cocultured with NT-T, CAR-T, or STAb-T cells at the indicated E:T ratios, and the expression of CD3 and BCMA was analyzed by flow cytometry. Graphs show the change over time in relative percentages of CD3$^+$BCMA$^-$, CD3$^-$BCMA$^+$, CD3$^-$BCMA$^-$, and CD3$^+$BCMA$^+$. Data are mean ± SD of two independent experiments (n = 2). (**H** and **I**) NT-T, CAR-T, or STAb-T cells were cocultured with U266^{Luc} target cells at a 1:1 E:T ratio in the presence of increasing concentrations of purified human BCMA-Fc fusion protein; after 48 hours, cytotoxic activity (H) and IFN-γ secretion (I) were analyzed. Data in (H) are mean ± SD of three independent experiments with duplicates (n = 6). Data in (I) are mean ± SD of two independent experiments with duplicates (n = 4). Significance was calculated by two-way ANOVA test corrected with a Tukey's multiple comparisons test. *P < 0.05, **P < 0.01, ***P < 0.001, ****P < 0.0001.

NT-T–treated mice and those receiving the lower number of CAR-T cells rapidly developed MM (Fig. 3, C to F). Mice treated with the higher number of CAR-T cells showed a delay in disease progression, with two mice being MM-free at endpoint (Fig. 3, C to F). In contrast, both STAb-T–treated groups were able to control disease progression, as evidenced by BLI, with only one mouse showing some tumor burden at weeks 5 and 6 in the TLD condition group (Fig. 3, C to F). Flow cytometry analysis of PB, BM, and spleen revealed complete disease control in both STAb-treated mice groups, except for one mouse in the TLD group (Fig. 3G), whereas a tumor infiltration in BM was observed in mice receiving CAR-T cells, especially in the TLD conditions (Fig. 3G). Regarding T cell expansion and persistence in STAb-treated mice, percentages of CD3$^+$ cells in PB and spleen were higher than those observed in the groups that received CAR-T cells (Fig. 3H). In both groups, the percentage of BCMA-CAR$^+$ and BCMA-TCE$^+$, calculated according to the expression of tdTo, ranged between 20 and 40% (Fig. 3I). Quantitative real-time reverse transcription polymerase chain reaction (qRT-PCR) confirmed the absence of BCMA-encoding transcripts (*Tnfrsf17*) in the BM of STAb-treated mice (molecular complete remission), except in one case, whereas the presence of *Tnfrsf17*-expressing tumor cells was confirmed in most CAR-T–treated mice

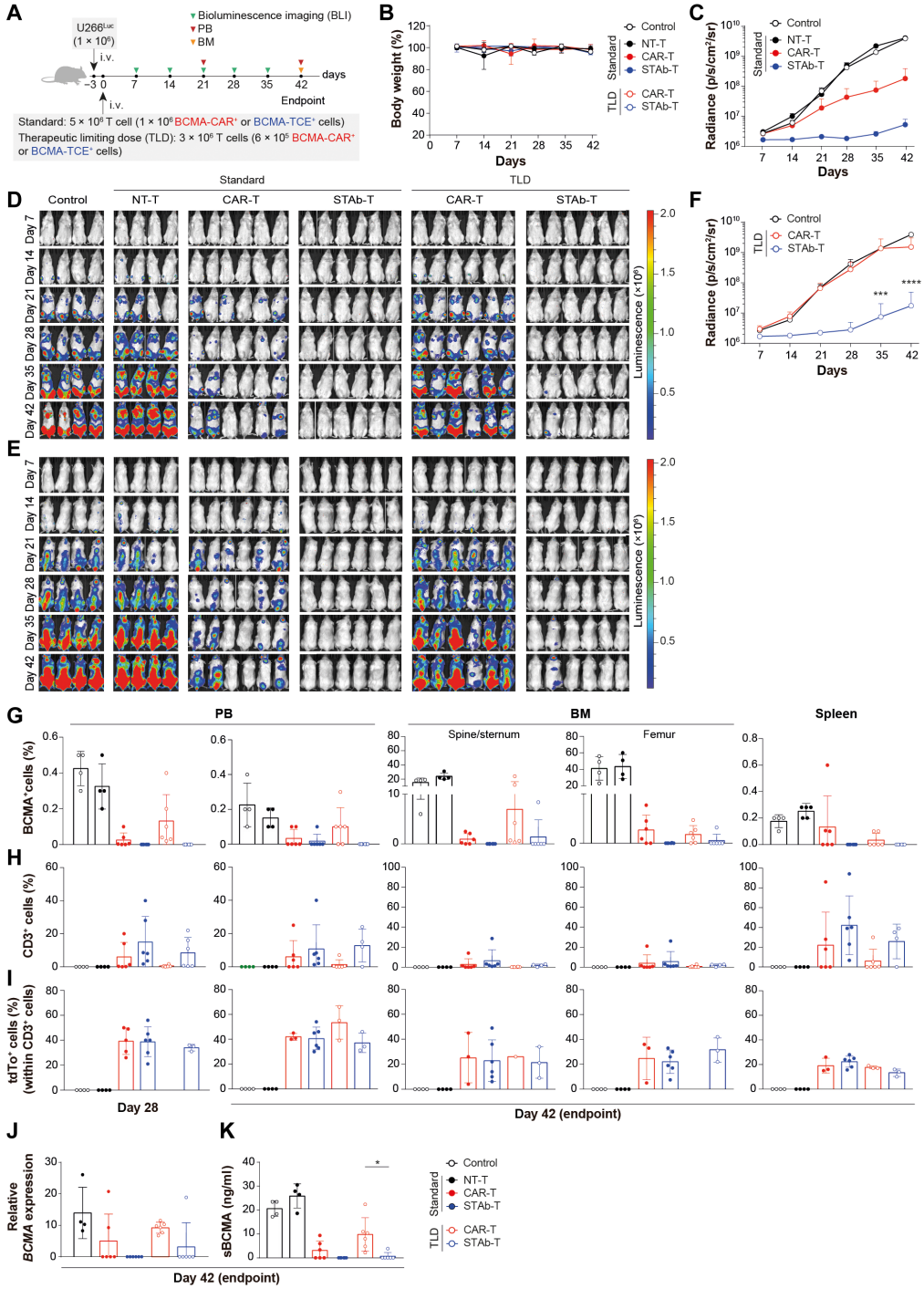

Fig. 3. STAb-T cells are more effective than CAR-T cells in a murine model of MM. (**A**) Study timeline. NSG mice received U266^{Luc} cells intravenously followed 3 days after by intravenous infusion of NT-T (5 × 10^6), CAR-T, or STAb-T cells [5 × 10^6 or 3 × 10^6, referred as standard and TLD model, respectively], accounting for 20% tdTo$^+$ T cells. (**B**) Change in body weight over time (%). (**C**) Radiance quantification (photons s^{-1} cm^{-2} sr^{-1}) in the standard model (control, NT-T, CAR-T, and STAb-T) at the indicated time points. Significance was calculated by two-way ANOVA test corrected with a Tukey's multiple comparisons test. (**D** and **E**) Bioluminescence images showing disease progression from ventral (D) and dorsal (E) views. (**F**) Radiance quantification in the TLD model (control, CAR-T, and STAb-T) at the indicated time points. Significance was calculated by two-way ANOVA test corrected with a Tukey's multiple comparisons test. (**G**) Detection by flow cytometry of MM cells (BCMA$^+$) cells in PB at day 28 and in PB, BM, and spleen at endpoint (day 42). (**H**) Detection by flow cytometry of CD3$^+$ T cells in PB at day 28 and in PB, BM, and spleen at endpoint (day 42). (**I**) Detection by flow cytometry of tdTo$^+$CD3$^+$ T cells in PB at day 28, and in PB, BM, and spleen at endpoint (day 42). (**J**) Relative *BCMA* mRNA expression in BM (spine/sternum) at endpoint. (**K**) Soluble BCMA (sBCMA) concentrations in plasma from mice at endpoint (day 42). Significance was calculated by two-way ANOVA test corrected with a Tukey's multiple comparisons test. *P < 0.05, **P < 0.01. Data are presented as mean ± SD of one experiment with six mice for CAR-T– and STAb-T–treated groups (n = 6), and four mice for NT-T and control groups (n = 4).

(Fig. 3J). These data were consistent with serum sBCMA concentrations, which were almost undetectable in mice receiving STAb-T cells, whereas concentrations of sBCMA were observed in both CAR groups, especially in the TLD condition (Fig. 3K).

STAb-T cell treatment promotes memory T cell formation in a murine MM model

To further characterize the in vivo–expanded STAb-T and CAR-T cells, we performed additional in vivo studies under TLD conditions, where NSG mice received intravenous injections of 3 × 10^6 NT-T, STAb-T, or CAR-T cells, with 20% of transduced (tdTo$^+$) TCE-BCMA$^+$ or CAR-BCMA$^+$ cells (Fig. 4A). NT-T– and CAR-T–treated mice rapidly developed MM, whereas STAb-T–treated mice were able to control disease progression (Fig. 4, B and C), which was consistent with the previous in vivo experiments (Fig. 3, C to F). At week 4, the mean percentage of CD3$^+$ cells in PB ranged from 4% in CAR-T–treated mice to 7% in mice receiving STAb-T cells (Fig. 4D). At this point, mice were euthanized, and BM and spleen samples were analyzed with a 30-antibody panel adapted for the simultaneous measurement of tdTo fluorescence and a fluorescein isothiocyanate (FITC)–labeled BCMA-Fc. The composition of the STAb-T and CAR-T preinfusion products was very similar, with only minor differences, such as higher percentage of effector CD4$^+$ T cells and a lower percentage of naïve CD4$^+$ T cells in both

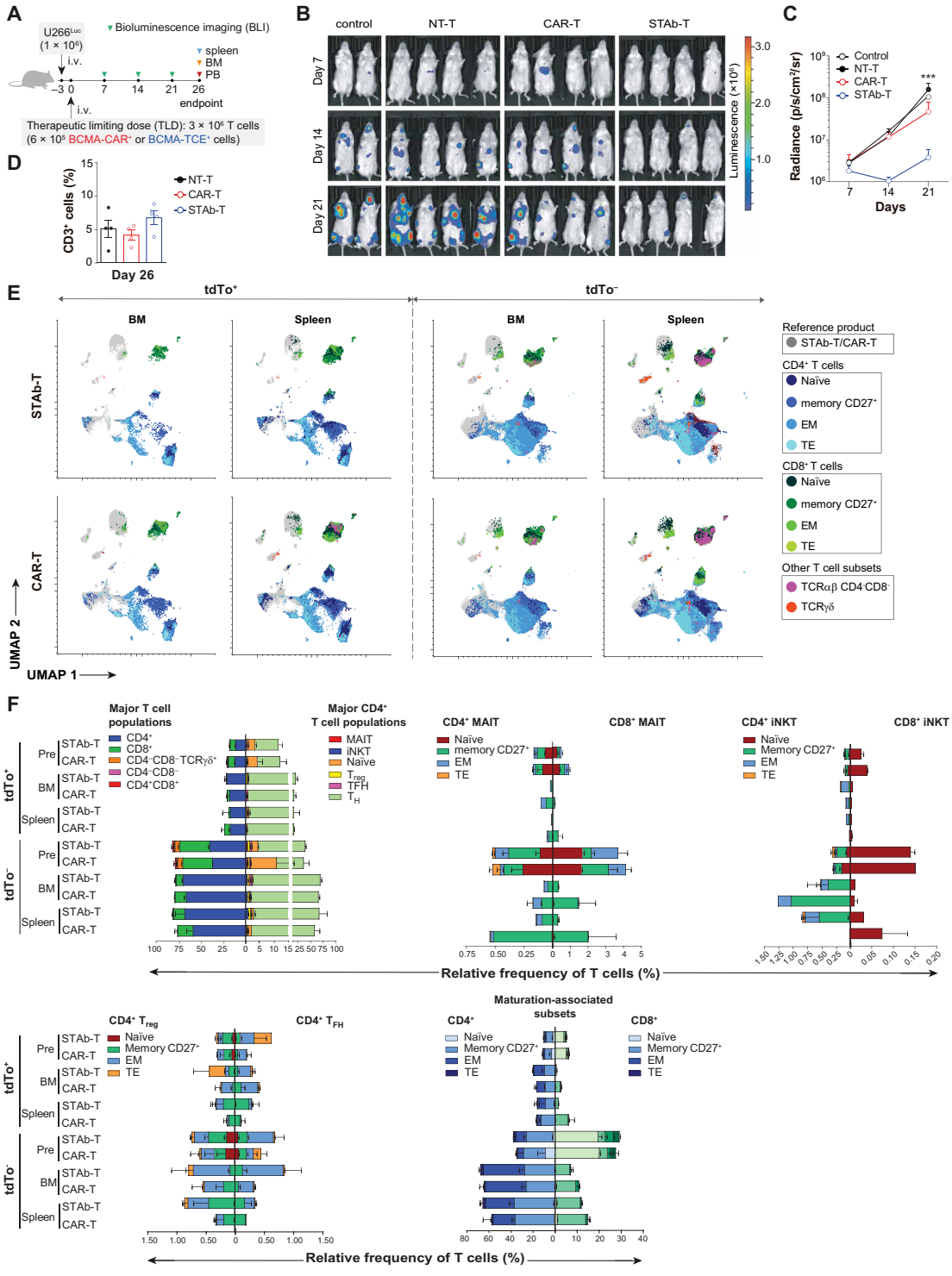

Fig. 4. STAb-T cell therapy is associated with memory T cell generation in a murine model of MM. (**A**) Study timeline. NSG mice received U266^{Luc} cells intravenously followed 3 days after by intravenous infusion of 3 × 10^6 NT-T CAR-T or STAb-T cells (TLD model), accounting for 20% tdTo$^+$ T cells. (**B**) Bioluminescence images showing disease progression from the ventral view. (**C**) Radiance quantification at the indicated time points. Significance was calculated by two-way ANOVA test corrected with a Tukey's multiple comparisons test. ***$P < 0.001$. (**D**) Detection by flow cytometry of CD3$^+$ T cells in PB at endpoint (day 26). Data in (C) and (D) are presented as median ± SD of one experiment with four mice for NT-T–, CAR-T–, and STAb-T–treated groups ($n = 4$) and two mice for control groups ($n = 2$). (**E** and **F**) UMAP (E) of the different T cell subsets identified in preinfusion STAb-T and CAR-T products (gray areas) overlaid with the corresponding (color-coded) BM and spleen from STAb-T– and CAR-T–treated mice classified according to the presence versus absence of tdTo expression and their relative numerical abundance (F). Data in (F) are presented as median ± SD of two independent pooled sample experiments. EM, effector memory; TE, terminal effector; MAIT, mucosal-associated invariant T cell; iNKT, invariant natural killer T cell; T_{reg}, regulatory T cell; T_{FH}, follicular helper T cell; T_H, (classical) T helper cell.

transduced ($tdTo^+$) and NT ($tdTo^-$) STAb-T cells (Fig. 4, E and F, and fig. S14). Among the $tdTo^+$ T cells recovered from the STAb-T–treated mice, an expansion of $CD4^+$ T cells, with predominance of memory phenotype $CD4^+$ T cells, was observed in both BM and spleen, without an increase of $CD4^+$ regulatory T cells (Fig. 4, E and F). In the NT $tdTo^-$ cells from the STAb-T preparation, a predominance of effector memory $CD4^+$ T cells was also observed, which may be attributable to the bystander effect of the secreted BCMA-TCE (Fig. 4, E and F). Among the in vivo–expanded CAR-T cells, the CD4:CD8 ratio of the preinfusion product was preserved because of a lower expansion of $CD4^+$ effector memory T cells and a higher percentage of memory $CD8^+$ T cells (Fig. 4, E and F). Collectively, this multimodal identification of T cell subsets in CAR-T and STAb-T cells expanded in vivo provides insights into the diversity of T cell responses after adoptive cell therapy with BCMA-specific CAR-T and STAb-T cells in MM.

DISCUSSION

Despite considerable progress, MM remains incurable with poor outcomes, particularly in patients with R/R MM, stressing the need for additional therapeutic approaches. Here, we demonstrate that engineered STAb-T cells secreting anti–BCMA-TCEs are more effective than state-of-the-art approved CAR-T cells engineered to express a second-generation 4-1BB–based anti-BCMA CAR at inducing specific cytotoxicity, preventing tumor escape in vitro, and inhibiting MM progression in vivo. CAR-T cells and bispecific TCEs are forefront T cell–redirecting strategies for cancer, but they differ in several key mechanistic aspects and have clinical pros and cons (*5*). TCE antibodies can recruit bystander T cells already present in the TME as effectors to kill MM cells (*35*). We demonstrated in both contact and noncontact coculture systems with $BCMA^+$ cells that STAb-T cells redirected bystander T cells, resulting in enhanced cytotoxic activity compared with that exhibited by CAR-T cells at very low E:T ratios. A further major mechanistic difference that affects the effector capacity of redirected T cells is related to the topology of the artificial immunological synapse induced by TCE and CAR. Data contributed by different publications show a noncanonical topology of the immunological synapse established by CAR-T cells (*29*, *34*, *36*, *37*). CAR-induced immunological synapses result in more transient early signaling and faster lymphocyte detachment from the target cell, which correlates with efficient repeat killing, at least at a high E:T ratio (5:1) (*36*). The comparison between CAR-T and STAb-T presented in this work indicates a proper early signaling, as measured by polarized pTyr abundance, slightly reduced F-actin polarization, and a lower hypodense area at the central supramolecular activation cluster of the CAR-induced immunological synapse. A lower F-actin polarization might indicate a reduced duration of the adhesion in the CAR-T cells. This should be further investigated by using live primary T cell imaging. A central hypodense actin network at the immunological synapse has been shown to be required for proper lytic granule secretion at the immunological synapse (*38*). Inadequate organization of central F-actin network might hamper the proper secretion of cytotoxic granules and, consequently, perturb the killing process, rendering therapies less effective as suggested by the in vitro and in vivo data reported here. The early signaling defects that render an inadequate depletion of F-actin at the secretory domain of the immunological synapse should be investigated.

In the context of systemically administered TCEs, the therapeutic effect is dependent on drug exposure, and it is rather unlikely for this T cell–redirecting strategy to generate a population of memory T cells responsible for long-term BCMA-specific responses after TCE withdrawal (*23*). In the STAb-T strategy, cells continuously secrete the TCE and display a stable quantity of BCMA-TCE decorating CD3 on the surface of T cells. The cis- and trans-decoration of CD3 results in specific adhesion to the targeted antigen almost as efficient as that observed with CAR-T cells (*29*), and our data demonstrate that this process contributes to the in vivo expansion and persistence of STAb-T cells, generating long-term antitumor responses, as has been reported for CAR-T cells (*22*, *35*). Our multimodal immunophenotypic studies with in vivo–expanded STAb-T and CAR-T cells revealed similar patterns with an expansion of memory populations. STAb-T cells showed a similar phenotypic profile within the $tdTo^+$ and $tdTo^-$ cell fractions, whereas, in CAR-T cells, minor changes were observed in $tdTo^-$ cells compared to $tdTo^+$ cells. This might be due to mechanistic differences between the strategies. STAb-T cells can secrete TCE efficiently despite being in an exhausted state after continued exposure to BCMA. This would ensure the sustained recruitment of nonactivated bystander T cells to ensure sustained anti-MM activity.

Escape mechanisms to CD19-targeted T cell–redirecting strategies have been documented experimentally and clinically in B cell acute lymphoblastic leukemia (B-ALL), leading to relapses with poor prognosis. Our previous work in B-ALL demonstrated that anti–CD19 STAb-T cells could prevent CD19 down-regulation and subsequent tumor escape more efficiently and at lower E:T ratios than CD19-specific CAR-T cells (*29*, *39*, *40*). As observed with CD1a-specific CAR-T and STAb-T cells in T-ALL (*30*), here, we did not observe loss of cell surface BCMA expression on MM cells cocultured with CAR-T or STAb-T cells, indicating that the down-regulation events depend on the targeted antigen and the phenotype and development plasticity of tumor cells. However, sBCMA has a completely different impact on the effector capacity of CAR-T and STAb-T cells. Concentrations ≥100 ng/ml affect the cytotoxic activity of CAR-T cells, whereas STAb-T cells do not reduce their cytotoxic capacity even at 50-fold higher concentrations of sBCMA. An additional advantage of STAb-T cells over CAR-T cells lies in the fact that STAb-T–based therapies might require lower doses of T cells, reducing the time required for product generation, which could be of relevance when sufficient numbers of T cells cannot be generated because of the lymphopenic state of some patients with R/R MM. The main limitation of our study is associated with the use of an immunodeficient mouse model. The use of humanized mice, or syngeneic mouse models, will allow better characterization of the impact of continuous secretion of BCMA-TCE by STAb-T cells on long-term antitumor responses and toxicity. An additional limitation of our studies is that they were conducted with tumor cell lines, and the results may not be directly translatable to the clinical setting because patients with R/R MM present considerable tumor heterogeneity. STAb-T–based immunotherapies could potentially benefit from strategies to overcome resistance to T cell–redirecting approaches, such as dual-targeting therapies.

In summary, anti–BCMA STAb-T cells may represent an alternative to current treatments for patients with R/R MM based on TCEs and CAR-T cells because they have certain advantages, such as the reduced impact of sBCMA on the BCMA-specific activation of STAb-T cells, as well as the continuous secretion of TCEs. This

allows for a rapid and efficient recruitment of the endogenous T cell pool in the TME and the expansion and persistence in vivo of memory STAb-T cells to generate long-term BCMA-specific responses.

MATERIALS AND METHODS

Study design

The study was designed to develop and characterize engineered T cells secreting BCMAxCD3 TCEs (STAb-T BCMA) and to conduct a comprehensive preclinical study comparing their therapeutic potential with T cells expressing anti-BCMA CARs (CAR-T BCMA) in a T cell–limiting experimental setting mimicking the conditions found in patients with R/R MM. We hypothesize that polyclonal recruitment of both genetically modified STAb-T cells and unmodified bystander T cells can substantially increase the control of MM progression. The study was performed with human MM cell lines and human primary MM cells and T cells. We used in vitro and in vivo models to evaluate the ability of STAb-T BCMA cells to prevent tumor scape and perform potent cytotoxic responses at low E:T ratios. Every experiment was performed comparing STAb-T BCMA cell activity to CAR-T BCMA. NT T cells were used as negative control. Sample sizes were determined on the basis of previous experiments and review of the literature. The number of biological (*n*) replicates is indicated in the figure legends. For in vivo experiments with NSG mice, animals were randomly assigned to each treatment group based on mean luminescent signal. Data analysis was performed in an unblinded manner.

Cell lines and culture conditions

Cell lines used are detailed in table S1. Cells were purchased from the American Type Culture Collection. The ARP1 cell line was provided by the Multiple Myeloma Research Center. Suspension cell lines were maintained in RPMI 1640 (catalog no. BE12-167F, Lonza) supplemented with 2 mM L-glutamine (catalog no. 25030081, Life Technologies), 10% (v/v) heat-inactivated fetal bovine serum (FBS) (catalog no. F7524), and penicillin-streptomycin (100 U/ml penicillin, 100 μg/ml streptomycin, catalog no. P4333), both from Sigma-Aldrich. Adherent cell lines were cultured in Dulbecco's modified Eagle's medium (DMEM) (catalog no. BE12-709F, Lonza) supplemented with 2 mM L-glutamine, 10% (v/v) heat-inactivated FBS, and penicillin/streptomycin. All the cell lines were grown at 37°C and 5% CO_2 and were routinely screened for mycoplasma contamination by PCR using the Mycoplasma Gel Detection Kit (catalog no. 90.021-4542, Biotools).

HEK293^{BCMA+} cell line generation

HEK293 cells were transfected with a pCMV3-BCMA-ORF vector including a hygromycin resistance marker for further cell selection (catalog no. SIB-HG10620-UT, Sino Biological). Cells were cultured in DMEM–10% FBS + hygromycin (150 μg/ml) (catalog no. 10687010, Thermo Fisher Scientific).

Vector construction

The pCCL–BCMA–4-1BB–CD3ζ–T2A–tdTo vector (BCMA-CAR) has been previously described and clinically validated (*20*). For the lentiviral vector pCCL-BCMA-OKT3-His-T2A-tdTo construction, the humanized anti-BCMA scFv (J22.9) (*20*) was subcloned in the pCDNA3.1 expression vector. OKT3-m/h26 from the pCR3.1-Ega1-OKT3 vector was subcloned as Not I/Xba I into the pcDNA3.1-hBCMA-ScFv vector, resulting in pCDNA3.1-BCMA-OKT3-m/h. To obtain the lentiviral vector pCCL-BCMA-OKT3-His-T2A-tdTo, a synthetic gene encoding the C-terminal polyHis (HHHHHH) tag, followed by 2A sequence from *Thosea asigna* virus (T2A) and the reporter red fluorescent protein tdTo, was synthesized by Geneart AG (Thermo Fisher Scientific), and the BCMA-OKT3–encoding fragment was subcloned as Bgl II/Bst BI in this vector. The whole fragment encoding BCMA-OKT3-His-T2A-tdTo was then subcloned into lentiviral pCCL vector as Bam HI/Bst BI to obtain the final pCCL-BCMA-OKT3-His-T2A-tdTo vector.

Lentiviral particle production and titration

To produce lentiviral particles for preclinical in vitro and in vivo studies, HEK293T cells were transfected with transfer vectors together with packaging plasmids pMDLg/pRRE (catalog no. PF1083, Plasmid Factory), pRSVrev (catalog no. PF1084, Plasmid Factory), and envelope plasmid pMD2.G (catalog no. PF096, Plasmid Factory), using linear polyethyleneimine of molecular weight 25,000 (catalog no. 23966-1, Polysciences). After 72 hours, viral supernatants were collected, clarified by centrifugation, filtrated using a 0.45-μm-pore filter, and ultracentrifuged for 2.5 hours at 26,000 rpm. Pellets containing the lentiviral particles were resuspended in RPMI 1640 (Lonza), aliquoted, and stored at −80°C until use. Functional titers of BCMA-TCE– and BCMA-CAR–encoding lentiviral vectors were determined by limiting dilution in Jurkat and HEK293T cells and analyzed using tdTo expression by flow cytometry.

T cell transduction

PBMCs were isolated from PB of volunteer healthy donors by density gradient centrifugation using Lymphoprep (catalog no. AXS-1114544, Axis-Shield). All donors provided written informed consent in accordance with the Declaration of Helsinki and approved by the Institutional Research Ethics Committees of the hospitals and research centers involved (HCB/2019/0450, HCB/2018/0030). Cells were activated with plate-coated anti-CD3 (1 μg/ml; OKT3 clone, catalog no. 566685, BD Biosciences) and plate-coated anti-CD28 (1 μg/ml; CD28.2 clone, catalog no. 555725, BD Biosciences) mAbs for 2 days and transduced at 10 or 20 (in vitro and in vivo assays, respectively) multiplicities of infection (MOIs) with BCMA CAR– or BCMA TCE–encoding lentiviral vectors in the presence of interleukin-7 (IL-7) (10 ng/ml; catalog no. 30-095-367, Miltenyi Biotec) and IL-15 (10 ng/ml; catalog no. 30-095-764 Miltenyi Biotec). As negative controls, NT primary T cells (NT-T) were used. A period of cell expansion of 6 to 8 days was carried out before conducting experiments. Jurkat T cells (1×10^5) were transduced with BCMA CAR– or BCMA TCE–encoding lentivirus at an MOI of 10. As negative controls, NT Jurkat T cells (J-NT-T) were used.

Flow cytometry

Antibodies used for flow cytometry analysis are detailed in table S2. Cell surface expression of BCMA-CAR was analyzed by incubation with recombinant human BCMA-Fc fusion protein (catalog no. RND-193-BC-050; R&D Systems) followed by incubation by Brilliant Violet (BV421)–conjugated anti-human immunoglobulin G (IgG)–Fc–specific antibody (catalog no. 410704; BioLegend); alternatively, it was estimated on the basis of tdTo fluorescent protein expression. BCMA-TCE surface decoration and intracellular expression was assessed using an allophycocyanin (APC)–conjugated anti-His mAb (catalog no. 130-119-782; Miltenyi Biotec); alternatively, it was

estimated on the basis of tdTo expression. Intracellular BCMA-TCE was detected using the Inside Stain Kit (catalog no. 130-090-477, Miltenyi Biotec) following the manufacturer's instructions. Cell acquisition was performed in a BD FACSCAnto II flow cytometer using BD FACSDiva software (BD Biosciences). Alternatively, a DxFlex flow cytometer (Beckman Coulter) was used. Analysis was performed using FlowJo V10 software (Tree Star).

Western blotting

Samples were separated under reducing conditions on 10 to 20% tris-glycine gels (catalog no. 250 XP10202BOX, Life Technologies), transferred onto polyvinylidene difluoride membranes (catalog no. IPVH00010, Merck Millipore), and probed with anti-His mAb (PentaHis, catalog no. 34650, Qiagen) (200 ng/ml), followed by incubation with horseradish peroxidase (HRP)–conjugated goat anti-mouse IgG, Fc specific (0.8 μg/ml) (catalog no. A2554, Sigma-Aldrich). For analysis of cell lysates, purified mouse anti-human CD247 (CD3ζ) (0.25 μg/ml, clone 8D3, catalog no. 551034, BD Biosciences) was added, followed by incubation with HRP-conjugated goat anti-mouse IgG (1:10,000 dilution, catalog no. A2554, Sigma-Aldrich). Visualization of protein bands was performed with Pierce ECL Western Blotting substrate (catalog no. 32132, Invitrogen) using a ChemiDoc MP Imaging System machine (Bio-Rad Laboratories), controlled by Image Lab Software (Bio-Rad Laboratories).

Enzyme-linked immunosorbent assay

To detect the BCMA-TCE secreted to cell culture supernatants, recombinant human BCMA-Fc chimera (catalog no. RND-193-BC-050, R&D Systems) was immobilized (3 μg/ml) on Maxisorp plates (catalog no. M9410-1CS, NUNC) overnight at 4°C. After washing and blocking, conditioned medium was added and incubated for 1 hour at room temperature. Then, wells were washed, and anti-His mAb (PentaHis, catalog no. 34650, Qiagen) was added (1 μg/ml) and incubated for 1 hour at room temperature. After washing, HRP-conjugated goat anti-mouse IgG, Fc specific (catalog no.1 15-085-166; Jackson Immunoresearch) was added (0.4 μg/ml) and incubated for 1 hour at room temperature, and then the plate was developed using tetramethylbenzidine (catalog no. T0440, Sigma-Aldrich). IFN-γ secretion was analyzed by enzyme-linked immunosorbent assay (ELISA; catalog no. 950.000.096; Diaclone) following the manufacturer's instructions. For sBCMA assessment in culture samples, the human BCMA/TNFRSF17 DuoSet ELISA kit (catalog no. DY193, R&D Systems) was used according to the manufacturer's instructions. Absorbance was read at 450- to 620-nm wavelengths using Multiscan Fc photometer (catalog no. 11500695, Thermo Fisher Scientific).

Cytotoxicity assays

For cytotoxicity assays, A-T cells, NT-T, CAR-T, or STAb-T, were cocultured with or without freshly isolated NA-T and luciferase-expressing tumor target cells ($U266^{Luc}$, $ARP1^{Luc}$, or $K562^{Luc}$) at the indicated E:T ratios. After 48 hours, supernatants were collected and stored at −20°C for further IFN-γ secretion analysis, and D-luciferin (catalog no. E1602, Promega) was added to cells to a final concentration of 20 μg/ml before bioluminescence quantification in relative light units using a Victor luminometer (PerkinElmer). The value for spontaneous lysis was obtained by incubating the target cells with NT-T or with NA-T effector cells only. Percent tumor cell viability was calculated as the mean bioluminescence of each sample divided by the mean bioluminescence of the input number of control target cells × 100. Specific lysis was established as 100% cell viability. For cytotoxic studies in noncontacting transwell systems, polycarbonate filter inserts (4.26 mm diameter) with 0.4-μm pores (catalog no. CLS3381-1EA; Corning) were used. In this experiment, luciferase-expressing targets cells (5×10^4) were plated on bottom wells with 5×10^4 NA-T cells (1:1 E:T ratio), and A-T cells (NT-T, CAR-T, or STAb-T cells) at the indicated ratios were added to transwell inserts. After 48 hours, bioluminescence was quantified as described. For cytotoxicity assays in the presence of sBCMA, $U266^{Luc}$ cells (5×10^4) were plated at 1:1 E:T ratio with 5×10^4 A-T cells (NT-T, CAR-T, or STAb-T), and increasing concentrations of recombinant human BCMA-Fc (catalog no. RND-193-BC-050; R&D Systems) were added in the culture medium (from 0 to 5 μg/ml). After 48 hours, bioluminescence was quantified as described above. For real-time cytotoxicity assays, the xCELLigence RTCA DP system (Acea BioSciences) was used. Wild-type HEK293 or stably transfected BCMA-expressing HEK293 cells ($HEK293^{BCMA+}$) (1×10^4) were plated in an E-Plate 16 (catalog no. 05469813001, Acea Biosciences) and cultured at 37°C and 5% CO_2. After 20 hours, NT-T, CAR-T BCMA, or STAb-T cells were added at different E:T ratios, and cell index values were measured every 15 min for 48 hours using RTCA Software 2.0 (Acea Biosciences). In another set of experiments, transduced (CAR-T or STAb-T) or NT-activated T cells were cocultured with primary MM BM cells or PBMCs from a patient diagnosed with an aggressive PCL at the indicated E:T ratios. After 24 hours, cells were stained for 30 min at 4°C with CD2–phycoerythrin (PE), CD3–PE–cyanine (Cy) 5.5, BCMA–Alexa Fluor 647, CD38-APC-Cy7, CD138-PE-Cy7, CD56-FITC, CD45-V500 (table S2), and 4′,6-diamidino-2-phenylindole (DAPI) (catalog no. D9542-10MG, Sigma-Aldrich) in 50 μl of PBS with 0.5% FBS in TruCount Absolute Counting Tubes (catalog no. 340334, BD Biosciences). Then, samples were diluted by adding 450 μl of PBS and gently mixed before flow cytometry analysis. Cell acquisition was performed in a DxFlex flow cytometer (Beckman Coulter) using FlowJo V10 software (Tree Star). Cytotoxicity was determined by analyzing the residual live (DAPI-negative) target cells.

Immunofluorescence and confocal microscopy

Jurkat effector T cells (J-NT-T, J-CAR-T, or J-STAb-T) were incubated at 37°C with U266 target cells at a E:T ratio of 1:1 for 15 min. As a positive control, a coculture of 1.5×10^5 J-NT-T cells and 1.5×10^5 Raji SEE-loaded cells [preincubated with 1 μM carboxyfluorescein diacetate succinimidyl ester (CFSE), catalog no. C34554, Thermo Fisher Scientific] were used. Jurkat/U266 conjugates (1.5×10^5 cells each) were fixed with 4% paraformaldehyde (Sigma-Aldrich) in PBS for 5 min at room temperature. Cells were then permeabilized with 0.1% Triton X-100 (Sigma-Aldrich) for 5 min at room temperature followed by blocking with human γ-globulin (10 μg/ml, catalog no. 345886, Sigma-Aldrich) for 20 min at room temperature. Samples were stained with the antibodies indicated in table S2 for 1 hour at room temperature. Then, cells were washed with tris-buffered saline (TBS) (20 mM tris and 150 mM NaCl) and incubated with Alexa Fluor 405 goat anti-rabbit antibody (catalog no. A31556, Thermo Fisher Scientific) (5 μg/ml) and phalloidin–Alexa Fluor 647 (1:300 dilution, catalog no. A22287, Thermo Fisher Scientific) at room temperature for 30 min. Last, the coverslips were washed twice with TBS and once with distilled water before being mounted with Mowiol medium. Confocal sections of fixed samples were

acquired using a Leica SP-8 confocal scanning laser microscopy with a 60×/1.35 oil immersion objective. Alexa Fluor 405 and phalloidin–Alexa Fluor 647 were excited with 405- and 633-nm laser lines, respectively. Image acquisition was automatically optimized with the Leica SP-8 confocal scanning laser microscopy software to get an image resolution of 58 nm per pixel. Analysis of images was conducted with ImageJ freeware (National Institutes of Health). The polarization of pTyr and F-actin at the immunological synapse was estimated with the Synapse Measure plugin of ImageJ. Actin clearance value from each individual synapse was calculated as the ratio between the central actin cleared area and the total area of the interface obtained from the three-dimensional (3D) reconstruction.

Xenograft animal model studies

NSG mice were irradiated (2 Gy) and infused intravenously with 1×10^6 $U266^{Luc}$ cells. After 3 days, mice were randomly allocated to six different groups and received either 5×10^6 or 3×10^6 NT-T, CAR-T (20% BCMA-CAR$^+$), or STAb-T (20% BCMA-TCE$^+$) cells. Tumor growth was evaluated weekly by BLI as previously described (*29*). Briefly, D-luciferin (150 mg/kg) (catalog no. E1605, Promega) was administrated intraperitoneally in 200 μl of sterile PBS. Animals were imaged 10 min after D-luciferin injection using the Xenogen IVIS Lumina II imaging system (Caliper Life Sciences). The photon flux emitted by the luciferase-expressing cells was measured as an average radiance (photons s^{-1} cm^{-2} sr^{-1}). In vivo studies were carried out at the Barcelona Biomedical Research Park (PRBB) in accordance with the guidelines of the Animal Experimentation Ethics Committee. All procedures were performed in compliance with the institutional animal care committee of the PRBB (DAAM9624). Tumor burden, T cell persistence, and % of tdTo$^+$ T cells in PB were analyzed by flow cytometry at day 28 or at the time of euthanasia. BM (spine/sternum and femur) and spleen samples were collected after euthanasia and analyzed by flow cytometry. Body weight was monitored over time. Animals showing endpoint clinical disease or signs of graft-versus-host disease were euthanized. Human *BCMA* relative gene expression in BM was analyzed by qRT-PCR. sBCMA was assessed in murine plasma samples collected at endpoint.

Quantitative real-time PCR

Total RNA from murine BM samples was isolated with the RNeasy Micro Kit (catalog no. 74004, Qiagen), and cDNA was synthesized using NZY First-Strand cDNA Synthesis Kit (catalog no. MB125, Nzytech). qRT-PCR was performed with LightCycler 480 SYBR Green I Master Kit (catalog no. 04707516001, Roche Diagnostics) on a LightCycler system (Roche Diagnostics). Each sample was analyzed in triplicate, and fold expression changes were calculated with the equation $2-\Delta Ct$. Human succinate dehydrogenase gene expression was used to normalize. The primers used (synthetized by Roche Diagnostics) are detailed in table S3.

Flow cytometric characterization of T lymphocyte subsets

Preinfused STAb-T and CAR-T cell products, whole BM, and spleen specimens from STAb-T–and CAR-T–treated mice were stained with the 30-color T cell module of the Euroflow-Immune monitoring antibody panel adapted for the simultaneous measurement of tdTo-associated fluorescence of both STAb-T and CAR-T cells and the FITC-labeled BCMA-Fc (catalog no. CD8-HF255, ACRO-Biosystems). Samples were labeled using the EuroFlow standard operating procedures for staining of cell surface membrane markers only (*41*), available at www.EuroFlow.org, plus the BCMA-FITC protein, aimed at simultaneous immunophenotypic identification of both transduced STAb-T (tdTo$^+$ BCMA-TCE$^+$) or CAR-T (tdTo$^+$ BCMA-CAR$^+$) cells and NT (tdTo$^-$) human T cells, and their most relevant maturation-associated and functional subsets (table S4). Stained samples were measured in a five-laser Aurora cell sorter (Aurora CS, Cytek Biosciences) using the SpectroFlo software (Cytek Biosciences). For data analysis and T cell subsetting (table S4), Infinicyt software (Cytognos SL) was used. UMAP (Uniform Manifold Approximation and Projection) plots of the various T cell subset profiles were built with the R (version 4.3.1) and the UWOT software packages (*42*).

Statistical analysis

Raw, individual-level data for experiments where $n < 20$ are presented in data file S1. Statistical analyses were performed with GraphPad Prism version 7 (GraphPad Prism Software). Significant differences from univariate analysis among three or more groups were determined by one- or two-way analysis of variance (ANOVA) followed by Tukey's multiple comparisons post hoc test. For bivariate analysis using a contingency table, statistical significance was calculated by Fisher's exact test. Specific test used in each experiment is indicated in the corresponding figure legend. Significance is defined as follows: $*P < 0.05$, $**P < 0.01$, $***P < 0.001$, and $****P < 0.0001$. Data are presented as the mean ± SD, and N represents the total number of technical and biological replicates performed.

Supplementary Materials

This PDF file includes:

Fig. S1 to S14
Tables S1 to S4
Legend for data file S1

Other Supplementary Material for this manuscript includes the following:

MDAR Reproducibility Checklist
Data file S1

REFERENCES AND NOTES

1. A. Palumbo, K. Anderson, Multiple myeloma. *N. Engl. J. Med.* **364**, 1046–1060 (2011).
2. S. V. Rajkumar, M. A. Dimopoulos, A. Palumbo, J. Blade, G. Merlini, M. V. Mateos, S. Kumar, J. Hillengass, E. Kastritis, P. Richardson, O. Landgren, B. Paiva, A. Dispenzieri, B. Weiss, X. LeLeu, S. Zweegman, S. Lonial, L. Rosinol, E. Zamagni, S. Jagannath, O. Sezer, S. Y. Kristinsson, J. Caers, S. Z. Usmani, J. J. Lahuerta, H. E. Johnsen, M. Beksac, M. Cavo, H. Goldschmidt, E. Terpos, R. A. Kyle, K. C. Anderson, B. G. Durie, J. F. Miguel, International Myeloma Working Group updated criteria for the diagnosis of multiple myeloma. *Lancet Oncol.* **15**, e538–e548 (2014).
3. P. Moreau, S. K. Kumar, J. S. Miguel, F. Davies, E. Zamagni, N. Bahlis, H. Ludwig, J. Mikhael, E. Terpos, F. Schjesvold, T. Martin, K. Yong, B. G. M. Durie, T. Facon, A. Jurczyszyn, S. Sidana, N. Raje, N. van de Donk, S. Lonial, M. Cavo, S. Y. Kristinsson, S. Lentzsch, R. Hajek, K. C. Anderson, C. João, H. Einsele, P. Sonneveld, M. Engelhardt, R. Fonseca, A. Vangsted, K. Weisel, R. Baz, V. Hungria, J. G. Berdeja, F. L. da Costa, A. Maiolino, A. Waage, D. H. Vesole, E. M. Ocio, H. Quach, C. Driessen, J. Bladé, X. Leleu, E. Riva, P. L. Bergsagel, J. Hou, W. J. Chng, U. H. Mellqvist, D. Dytfeld, J. L. Harousseau, H. Goldschmidt, J. Laubach, N. C. Munshi, F. Gay, M. Beksac, L. J. Costa, M. Kaiser, P. Hari, M. Boccadoro, S. Z. Usmani, S. Zweegman, S. Holstein, O. Sezer, S. Harrison, H. Nahi, G. Cook, M. V. Mateos, S. V. Rajkumar, M. A. Dimopoulos, P. G. Richardson, Treatment of relapsed and refractory multiple myeloma: Recommendations from the International Myeloma Working Group. *Lancet Oncol.* **22**, e105–e118 (2021).
4. U. H. Gandhi, R. F. Cornell, A. Lakshman, Z. J. Gahvari, E. McGehee, M. H. Jagosky, R. Gupta, W. Varnado, M. A. Fiala, S. Chhabra, E. Malek, J. Mansour, B. Paul, A. Barnstead, S. Kodali, A. Neppalli, M. Liedtke, S. Narayana, K. N. Godby, Y. Kang, A. Kansagra, E. Umyarova, E. C. Scott, P. Hari, R. Vij, S. Z. Usmani, N. S. Callander, S. K. Kumar, L. J. Costa, Outcomes of

patients with multiple myeloma refractory to CD38-targeted monoclonal antibody therapy. *Leukemia* **33**, 2266–2275 (2019).
5. B. Blanco, M. Compte, S. Lykkemark, L. Sanz, L. Alvarez-Vallina, T cell-redirecting strategies to 'STAb' tumors: Beyond CARs and bispecific antibodies. *Trends Immunol.* **40**, 243–257 (2019).
6. A. Lakshman, S. K. Kumar, Chimeric antigen receptor T-cells, bispecific antibodies, and antibody-drug conjugates for multiple myeloma: An update. *Am. J. Hematol.* **97**, 99–118 (2022).
7. A. Tapia-Galisteo, L. Álvarez-Vallina, L. Sanz, Bi- and trispecific immune cell engagers for immunotherapy of hematological malignancies. *J. Hematol. Oncol.* **16**, 83 (2023).
8. Y. Sasaki, S. Casola, J. L. Kutok, K. Rajewsky, M. Schmidt-Supprian, TNF family member B cell-activating factor (BAFF) receptor-dependent and -independent roles for BAFF in B cell physiology. *J. Immunol.* **173**, 2245–2252 (2004).
9. J. R. Darce, B. K. Arendt, S. K. Chang, D. F. Jelinek, Divergent effects of BAFF on human memory B cell differentiation into Ig-secreting cells. *J. Immunol.* **178**, 5612–5622 (2007).
10. L. Sanchez, A. Dardac, D. Madduri, S. Richard, J. Richter, B-cell maturation antigen (BCMA) in multiple myeloma: The new frontier of targeted therapies. *Ther. Adv. Hematol.* **12**, 2040620721989585 (2021).
11. R. O. Carpenter, M. O. Evbuomwan, S. Pittaluga, J. J. Rose, M. Raffeld, S. Yang, R. E. Gress, F. T. Hakim, J. N. Kochenderfer, B-cell maturation antigen is a promising target for adoptive T-cell therapy of multiple myeloma. *Clin. Cancer Res.* **19**, 2048–2060 (2013).
12. N. W. C. J. van de Donk, S. Z. Usmani, K. Yong, CAR T-cell therapy for multiple myeloma: State of the art and prospects. *Lancet Haematol.* **8**, e446–e461 (2021).
13. R. Firestone, A. M. Lesokhin, S. Z. Usmani, An embarrassment of riches: Three FDA-approved bispecific antibodies for relapsed refractory multiple myeloma. *Blood Cancer Discov.* **4**, 433–436 (2023).
14. N. C. Munshi, L. D. Anderson, N. Shah, D. Madduri, J. Berdeja, S. Lonial, N. Raje, Y. Lin, D. Siegel, A. Oriol, P. Moreau, I. Yakoub-Agha, M. Delforge, M. Cavo, H. Einsele, H. Goldschmidt, K. Weisel, A. Rambaldi, D. Reece, F. Petrocca, M. Massaro, J. N. Connarn, S. Kaiser, P. Patel, L. Huang, T. B. Campbell, K. Hege, J. San-Miguel, Idecabtagene vicleucel in relapsed and refractory multiple myeloma. *N. Engl. J. Med.* **384**, 705–716 (2021).
15. T. Martin, S. Z. Usmani, J. G. Berdeja, M. Agha, A. D. Cohen, P. Hari, D. Avigan, A. Deol, M. Htut, A. Lesokhin, N. C. Munshi, E. O'Donnell, A. K. Stewart, J. M. Schecter, J. D. Goldberg, C. C. Jackson, T. M. Yeh, A. Banerjee, A. Allred, E. Zudaire, W. Deraedt, Y. Olyslager, C. Zhou, L. Pacaud, D. Madduri, A. Jakubowiak, Y. Lin, S. Jagannath, Ciltacabtagene autoleucel, an anti-B-cell maturation antigen chimeric antigen receptor t-cell therapy, for relapsed/refractory multiple myeloma: CARTITUDE-1 2-year follow-Up. *J. Clin. Oncol.* **41**, 1265–1274 (2023).
16. A. Oliver-Caldés, V. González-Calle, V. Cabañas, M. Español-Rego, P. Rodríguez-Otero, J. L. Reguera, L. López-Corral, B. Martin-Antonio, A. Zabaleta, S. Inogés, S. Varea, L. Rosiñol, A. López-Díaz de Cerio, N. Tovar, R. Jiménez, M. López-Parra, L. G. Rodríguez-Lobato, A. Sánchez-Salinas, E. Olesti, M. Calvo-Orteu, J. Delgado, J. A. Pérez-Simón, B. Paiva, F. Prósper, J. Sáez-Peñataro, M. Juan, J. M. Moraleda, M. V. Mateos, M. Pascal, A. Urbano-Ispizua, C. Fernández de Larrea, Fractionated initial infusion and booster dose of ARI0002h, a humanised, BCMA-directed CAR T-cell therapy, for patients with relapsed or refractory multiple myeloma (CARTBCMA-HCB-01): A single-arm, multicentre, academic pilot study. *Lancet Oncol.* **24**, 913–924 (2023).
17. P. Moreau, A. L. Garfall, N. W. C. J. van de Donk, H. Nahi, J. F. San-Miguel, A. Oriol, A. K. Nooka, T. Martin, L. Rosinol, A. Chari, L. Karlin, L. Benboubker, M. V. Mateos, N. Bahlis, R. Popat, B. Besemer, J. Martínez-López, S. Sidana, M. Delforge, L. Pei, D. Trancucci, R. Verona, S. Girgis, S. X. W. Lin, Y. Olyslager, M. Jaffe, C. Uhlar, T. Stephenson, R. Van Rampelbergh, A. Banerjee, J. D. Goldberg, R. Kobos, A. Krishnan, S. Z. Usmani, Teclistamab in relapsed or refractory multiple myeloma. *N. Engl. J. Med.* **387**, 495–505 (2022).
18. A. M. Lesokhin, M. H. Tomasson, B. Arnulf, N. J. Bahlis, H. Miles Prince, R. Niesvizky, P. Rodríguez-Otero, J. Martinez-Lopez, G. Koehne, C. Touzeau, Y. Jethava, H. Quach, J. Depaus, H. Yokoyama, A. E. Gabayan, D. A. Stevens, A. K. Nooka, S. Manier, N. Raje, S. Iida, M. S. Raab, E. Searle, E. Leip, S. T. Sullivan, U. Conte, M. Elmeliegy, A. Czibere, A. Viqueira, M. Mohty, Elranatamab in relapsed or refractory multiple myeloma: Phase 2 MagnetisMM-3 trial results. *Nat. Med.* **29**, 2259–2267 (2023).
19. E. Sanchez, M. Li, A. Kitto, J. Li, C. S. Wang, D. T. Kirk, O. Yellin, C. M. Nichols, M. P. Dreyer, C. P. Ahles, A. Robinson, E. Madden, G. N. Waterman, R. A. Swift, B. Bonavida, R. Boccia, R. A. Vescio, J. Crowley, H. Chen, J. R. Berenson, Serum B-cell maturation antigen is elevated in multiple myeloma and correlates with disease status and survival. *Br. J. Haematol.* **158**, 727–738 (2012).
20. L. Perez-Amill, G. Suñe, A. Antoñana-Vildosola, M. Castella, A. Najjar, J. Bonet, N. Fernández-Fuentes, S. Inogés, A. López, C. Bueno, M. Juan, Á. Urbano-Ispizua, B. Martín-Antonio, Preclinical development of a humanized chimeric antigen receptor against B cell maturation antigen for multiple myeloma. *Haematologica* **106**, 173–184 (2021).
21. K. Pillarisetti, G. Powers, L. Luistro, A. Babich, E. Baldwin, Y. Li, X. Zhang, M. Mendonça, N. Majewski, R. Nanjunda, D. Chin, K. Packman, Y. Elsayed, R. Attar, F. Gaudet, Teclistamab is an active T cell-redirecting bispecific antibody against B-cell maturation antigen for multiple myeloma. *Blood Adv.* **4**, 4538–4549 (2020).
22. R. G. Majzner, C. L. Mackall, Clinical lessons learned from the first leg of the CAR T cell journey. *Nat. Med.* **25**, 1341–1355 (2019).
23. H. Benonisson, I. Altıntaş, M. Sluijter, S. Verploegen, A. F. Labrijn, D. H. Schuurhuis, M. A. Houtkamp, J. S. Verbeek, J. Schuurman, T. van Hall, CD3-bispecific antibody therapy turns solid tumors into inflammatory sites but does not install protective memory. *Mol. Cancer Ther.* **18**, 312–322 (2019).
24. B. Blanco, A. Ramirez-Fernandez, L. Alvarez-Vallina, Engineering immune cells for in vivo secretion of tumor-specific T cell-redirecting bispecific antibodies. *Front. Immunol.* **11**, 1792 (2020).
25. B. Blanco, P. Holliger, R. G. Vile, L. Alvarez-Vallina, Induction of human T lymphocyte cytotoxicity and inhibition of tumor growth by tumor-specific diabody-based molecules secreted from gene-modified bystander cells. *J. Immunol.* **171**, 1070–1077 (2003).
26. M. Compte, B. Blanco, F. Serrano, A. M. Cuesta, L. Sanz, A. Bernad, P. Holliger, L. Alvarez-Vallina, Inhibition of tumor growth in vivo by in situ secretion of bispecific anti-CEA x anti-CD3 diabodies from lentivirally transduced human lymphocytes. *Cancer Gene Ther.* **14**, 380–388 (2007).
27. M. Compte, A. Alvarez-Cienfuegos, N. Nuñez-Prado, N. Sainz-Pastor, A. Blanco-Toribio, N. Pescador, L. Sanz, L. Alvarez-Vallina, Functional comparison of single-chain and two-chain anti-CD3-based bispecific antibodies in gene immunotherapy applications. *Oncoimmunology* **3**, e28810 (2014).
28. M. Compte, A. M. Cuesta, D. Sánchez-Martín, V. Alonso-Camino, J. L. Vicario, L. Sanz, L. Alvarez-Vallina, Tumor immunotherapy using gene-modified human mesenchymal stem cells loaded into synthetic extracellular matrix scaffolds. *Stem Cells* **27**, 753–760 (2009).
29. B. Blanco, Á. Ramírez-Fernández, C. Bueno, L. Argemí-Muntadas, P. Fuentes, Ó. Aguilar-Sopeña, F. Gutierrez-Agüera, S. R. Zanetti, A. Tapia-Galisteo, L. Díez-Alonso, A. Segura-Tudela, M. Castellà, B. Marzal, S. Betriu, S. L. Harwood, M. Compte, S. Lykkemark, A. Erce-Llamazares, L. Rubio-Pérez, A. Jiménez-Reinoso, C. Domínguez-Alonso, M. Neves, P. Morales, E. Paz-Artal, S. Guedan, L. Sanz, M. L. Toribio, P. Roda-Navarro, M. Juan, P. Menéndez, L. Álvarez-Vallina, Overcoming CAR-mediated CD19 downmodulation and leukemia relapse with T lymphocytes secreting anti-CD19 T-cell engagers. *Cancer Immunol. Res.* **10**, 498–511 (2022).
30. A. Jiménez-Reinoso, N. Tirado, A. Martinez-Moreno, V. M. Díaz, M. García-Peydró, O. Hangiu, L. Díez-Alonso, Á. Albitre, P. Penela, M. L. Toribio, P. Menéndez, L. Álvarez-Vallina, D. Sánchez Martínez, Efficient preclinical treatment of cortical T cell acute lymphoblastic leukemia with T lymphocytes secreting anti-CD1a T cell engagers. *J. Immunother. Cancer* **10**, e005333 (2022).
31. X. Liu, D. M. Barrett, S. Jiang, C. Fang, M. Kalos, S. A. Grupp, C. H. June, Y. Zhao, Improved anti-leukemia activities of adoptively transferred T cells expressing bispecific T-cell engager in mice. *Blood Cancer J.* **6**, e430 (2016).
32. M. P. Velasquez, D. Torres, K. Iwahori, S. Kakarla, C. Arber, T. Rodriguez-Cruz, A. Szoor, C. L. Bonifant, C. Gerken, L. J. Cooper, X. T. Song, S. Gottschalk, T cells expressing CD19-specific engager molecules for the immunotherapy of CD19-positive malignancies. *Sci. Rep.* **6**, 27130 (2016).
33. F. Oden, S. F. Marino, J. Brand, S. Scheu, C. Kriegel, D. Olal, A. Takvorian, J. Westermann, B. Yilmaz, M. Hinz, O. Daumke, U. E. Höpken, G. Müller, M. Lipp, Potent anti-tumor response by targeting B cell maturation antigen (BCMA) in a mouse model of multiple myeloma. *Mol. Oncol.* **9**, 1348–1358 (2015).
34. Á. Ramírez-Fernández, Ó. Aguilar-Sopeña, L. Díez-Alonso, A. Segura-Tudela, C. Domínguez-Alonso, P. Roda-Navarro, L. Álvarez-Vallina, B. Blanco, Synapse topology and downmodulation events determine the functional outcome of anti-CD19 T cell-redirecting strategies. *Oncoimmunology* **11**, 2054106 (2022).
35. D. J. DiLillo, K. Olson, K. Mohrs, T. C. Meagher, K. Bray, O. Sineshchekova, T. Startz, J. Kuhnert, M. W. Retter, S. Godin, P. Sharma, F. Delfino, J. Lin, E. Smith, G. Thurston, J. R. Kirshner, A BCMAxCD3 bispecific T cell-engaging antibody demonstrates robust antitumor efficacy similar to that of anti-BCMA CAR T cells. *Blood Adv.* **5**, 1291–1304 (2021).
36. A. J. Davenport, R. S. Cross, K. A. Watson, Y. Liao, W. Shi, H. M. Prince, P. A. Beavis, J. A. Trapani, M. H. Kershaw, D. S. Ritchie, P. K. Darcy, P. J. Neeson, M. R. Jenkins, Chimeric antigen receptor T cells form nonclassical and potent immune synapses driving rapid cytotoxicity. *Proc. Natl. Acad. Sci. U.S.A.* **115**, E2068–E2076 (2018).
37. P. Roda-Navarro, L. Álvarez-Vallina, Understanding the spatial topology of artificial immunological synapses assembled in t cell-redirecting strategies: A major issue in cancer immunotherapy. *Front. Cell Dev. Biol.* **7**, 370 (2020).
38. T. Douanne, G. M. Griffiths, Cytoskeletal control of the secretory immune synapse. *Curr. Opin. Cell Biol.* **71**, 87–94 (2021).
39. R. Gardner, D. Wu, S. Cherian, M. Fang, L. A. Hanafi, O. Finney, H. Smithers, M. C. Jensen, S. R. Riddell, D. G. Maloney, C. J. Turtle, Acquisition of a CD19-negative myeloid

phenotype allows immune escape of MLL-rearranged B-ALL from CD19 CAR-T-cell therapy. *Blood* **127**, 2406–2410 (2016).
40. F. Braig, A. Brandt, M. Goebeler, H. P. Tony, A. K. Kurze, P. Nollau, T. Bumm, S. Böttcher, R. C. Bargou, M. Binder, Resistance to anti-CD19/CD3 BiTE in acute lymphoblastic leukemia may be mediated by disrupted CD19 membrane trafficking. *Blood* **129**, 100–104 (2017).
41. T. Kalina, J. Flores-Montero, V. H. J. van der Velden, M. Martin-Ayuso, S. Böttcher, M. Ritgen, J. Almeida, L. Lhermitte, V. Asnafi, A. Mendonça, R. de Tute, M. Cullen, L. Sedek, M. B. Vidriales, J. J. Pérez, J. G. te Marvelde, E. Mejstrikova, O. Hrusak, T. Szczepański, J. J. M. van Dongen, A. Orfao, EuroFlow Consortium (EU-FP6, LSHB-CT-2006-018708), EuroFlow standardization of flow cytometer instrument settings and immunophenotyping protocols. *Leukemia* **26**, 1986–2010 (2012).
42. L. M. Innes, J. Healy, J. Melville, UMAP: Uniform Manifold Approximation and Projection for dimension reduction. arXiv:1802.03426 [stat.ML] (2020).

Acknowledgments: We would like to thank the Cell Sorting Service of the NUCLEUS platform (University of Salamanca, Salamanca, Spain) for technical assistance. **Funding:** Financial support for this work was obtained from the Spanish Ministry of Science and Innovation MCIN/AEI/10.13039/501100011033 (PID2020-115444GB-I00 to P.R.-N., PID2019-108160RB-I00 to P.M., PLE2021-0075 to C.B., and PID2020-117323RB-100 and PDC2021-121711-100 to L.Á.-V.), partially supported by the European Regional Development Fund (ERDF); the Carlos III Health Institute (ISCIII) (PI20/01030 to B.B., PI19/00132 to L.S., PI21-01834 to P.P., PI20/00822 to C.B., and DTS20/00089 to L.Á.-V.), partially supported by the ERDF; the ISCIII-RICORS within the Next Generation EU program (plan de Recuperación, Transformación y Resilencia) (RD21/0017/0030 to B.B. and J.M.-L. and RD21/0017/0029 to P.M.); the ISCIII-CIBERONC program (CB16/12/00400 to A.O.), the CRIS Cancer Foundation (FCRIS-2021-001 to J.M.-L. and FCRIS-2021-0090 to L.Á.-V.), the Spanish Association Against Cancer (AECC) (PRYGN234975MENE to P.M., PRYGN211192BUEN to C.B., and PROYE19084ALVA and PRYGN234844ALVA to L.Á.-V.); the Accelerator Award-Cancer Research UK/AIRC/AECC-INCAR (GEACC18001ORF to A.O.), the Fundación "La Caixa" (LCF/PR/HR19/52160011 to P.M. and HR21-00761 project IL7R_LungCan to L.Á.-V.), the European Research Council (ERC) (ERC-PoC-957466 to P.M.) and ERC under the EU's Horizon Program (grant agreement 101100665 to P.M.), the Fundación de Investigación Biomédica 12 de Octubre (programa Investiga 2022-0082) to L.Á.-V.; the Fundación Ramón Areces to P.P. L.D.-A. was supported by a Rio Hortega fellowship from the Carlos III Health Institute (CM20/00004). A.F. was supported by a postdoctoral fellowship from the Spanish Ministry of Science and Innovation (FJC2021-046789-I). A. Mayado was supported by the CIBERONC (PRF-2869). A.P.-P. was supported by a grant from the Government of Castilla y León (Orden EDU/556/2019; Valladolid, Spain). M.G.-R. was supported by an industrial PhD fellowship from the Comunidad de Madrid (IND2022/BMD-23732). O.A.-S. was supported by a PhD fellowship from the Complutense University of Madrid. C.D.-A. was supported by a PhD fellowship from the Spanish Ministry of Science and Innovation (PRE2018-083445). L.R.-P. was supported by a PhD fellowship from the Immunology Chair, Universidad Francisco de Vitoria/Merck. O.H. was supported by an industrial PhD fellowship from the Comunidad de Madrid (IND2020/BMD-17668). A.V. is supported by Research Institute Hospital 12 de Octubre (imas12). A.G.-O. is supported by HIGEA 2019/0123 AIE project to J.M.-L. **Author contributions:** B.M.-A., P.M., C.B., and L.Á.-V. conceptualized and designed the study. M. Juan, B.M.-A., A.O., P.M., C.B., and L.Á.-V. developed methodology. L.D.-A., A.F., J.A.-R., P.A.R., A. Martínez, B.B., A.J.-R., A. Mayado, A.P.-P., M.G.-R., O.A.-S., A.R.-F., A.S.-T., L.P.-A., A.T.-G., C.D.-A., L.R.-P., M. Jara, F.S., O.H., L.A., A.A., P.P., L.S., E.A., A.V., A.G.-O., P.R., M. Juan, J.M.-L., P.R.-N., B.M.-A., P.M., C.B., and L.Á.-V. acquired, analyzed, and interpreted data. L.Á.-V. supervised the study. L.D.-A., B.B., A.J.-R., A.V., M. Juan, J.M.-L., P.R.-N., B.M.-A., A.O., P.M., C.B., and L.Á.-V. wrote, reviewed, or revised the manuscript. **Competing interests:** B.B., J.M.-L., and L.Á.-V. are cofounders of STAb Therapeutics, a spin-off company from the Instituto de Investigación Sanitaria Hospital 12 de Octubre (imas12). B.B., M. Juan, and L.Á.-V. are inventors on the patent application "Anti-CD19/anti-CD3 bispecific antibody, T cells secreting the same, method of preparation and use thereof" (EP21708942). L.D.-A., B.M.-A., M. Juan, and L.Á.-V. are inventors on the patent application "T cells expressing anti-BCMA/anti-CD3 antibodies and uses thereof" (EP23383410.0). B.M.-A., L.P.-A., and M. Juan are inventors on the patent application "CAR T-cells against BCMA for the treatment of multiple myeloma" (EP4007777A1). L.Á.-V. is cofounder of Leadartis, a spin-off focused on an unrelated interest. P.M. is cofounder of OneChain Immunotherapeutics, a spin-off company from the Josep Carreras Leukemia Research Institute. P.R. has licensed medicinal products and receives research funding and equity from Rocket Pharmaceuticals Inc. P.R. is an inventor on the following patent applications: "Methods for gene modification of hematopoietic cells" (PCT/US2019/044237) and "Gene therapy for patients with Fanconi anemia" (PCT/US2017/050837). L.P.-A. is currently an employee of Gyala Therapeutics, a spin-off focused on CAR-T cell products. **Data and materials availability:** All data associated with this study are present in the paper or the Supplementary Materials. UMAP data presented in Fig. 4 and fig. S14 were deposited in Dryad with the following DOI: 10.5061/dryad.83bk3jb04. Materials can be obtained after completion of a material transfer agreement with CNIO. Requests should be submitted to iherrera@cnio.es.

Submitted 21 January 2023
Resubmitted 13 November 2023
Accepted 2 January 2024
Published 14 February 2024
10.1126/scitranslmed.adg7962